Experiments in Fluids (2023) 64:129
https://doi.org/10.1007/s00348-023-03670-3

RESEARCH ARTICLE

Controlling upwards and downwards gust loads on aerofoils by pitching

I. Andreu-Angulo[1] · **H. Babinsky**[1]

Received: 21 January 2023 / Revised: 9 June 2023 / Accepted: 16 June 2023 / Published online: 7 July 2023

Abstract
A wing travelling at a constant angle of attack, α, experiences a large lift spike when subjected to a high-amplitude transverse gust. This study analyses the capability of a low-order model, which uses Wagner and Küssner theory, to calculate a pitch motion profile that mitigates such a lift increase. The model's pitch profiles are tested experimentally by towing a wing at a constant α towards a top-hat transverse gust. Throughout the gust encounter, the wing is pitched with a profile predetermined by the model. Force and flow measurements are analysed for gust ratios of 0.5 and 1.0 and angles of attack of 0, 10, 20 and 45 degrees. In addition, two gust directions are analysed: upwards where the gust velocity is in the direction of positive lift, and downwards (in the opposite direction). The latter produces a large negative lift spike that can be especially dangerous for flying vehicles. Experimental results demonstrate strong mitigation, around 85%, of the gust loads up to an effective angle of attack of 60 degrees, independently of gust direction. The theories used achieve mitigation even at large perturbations and separated flows, where the assumptions used on their derivation are clearly invalid. The mitigation approach does, nevertheless, not mitigate the secondary lift peak that emerges after gust exit when the initial wing incidence exceeds 10 degrees. This secondary peak is a result of attached flow around the wing right after gust exit, which eventually develops into a LEV that sheds from the wing.

1 Introduction

Aircraft experience adverse unsteady atmospheric conditions (Watkins et al. 2006) as a consequence of terrain roughness and temperature changes (Fuller 2008). These wind-vehicle interactions can result in sudden large loads, which become more extreme as the ratio of gust velocity to flight velocity increases, $GR = v_g/U$. In addition, when GR approaches 1 significant vorticity is shed into the flow during the gust encounter. Gusts can affect the vehicle from any direction. Downwards gusts are especially dangerous due to the rapid reduction in lift deriving from them (Roberts and Hunt 1968). Strong unsteady wing-gust interactions are particularly common in micro air vehicles, MAVs, due to their low flight speeds, as illustrated in Fig. 1. In order to fly these vehicles safely in a large range of atmospheric conditions, it is necessary to have a strong control mechanism. In many cases, controls are used to make adjustments that correct deviations from the prescribed course. However, reacting to changes in the vehicle attitude may be insufficient for extreme gust loads, where loads are large and sudden. In this paper, we will study how an aerodynamic model can be used to preemptively calculate the gust mitigation approach in wings flying at intermediate angles of attack and encountering upwards and downwards gusts.

There are only a limited number of studies on the mitigation of the large force peak observed by (Corkery et al. 2018; Biler et al. 2019) when a wing experiences high-amplitude gusts. Many of these mitigation studies are confined to upwards gusts and based solely on observations of the flight of birds and insects, where changes to the wing kinematics are often successful at reducing unsteady loads and their effects on the flight trajectory. For example, asymmetric wing strokes on bees have been shown to alleviate gusts with GR of order one (Vance et al. 2013). Owls use wing motion as a suspension system to passively mitigate gusts (Cheney et al. 1937). Wing actuation can create large and diverse loads without requiring any additional devices. For these reasons, we are exploiting the potential of simple wing motions to mitigate gust forces.

✉ I. Andreu-Angulo
ia347@cam.ac.uk

[1] Department of Engineering, University of Cambridge, Trumpington Street, Cambridge CB2 1PZ, UK

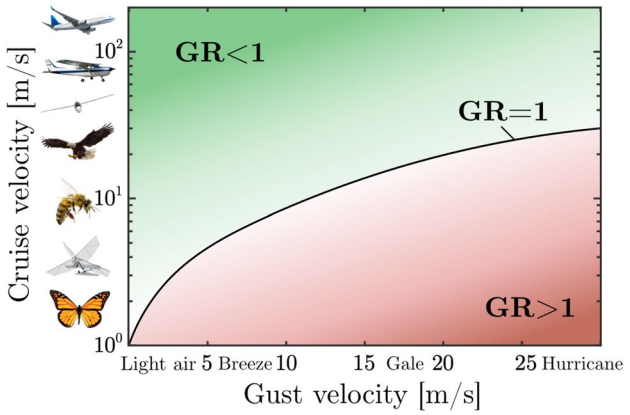

Fig. 1 Gust ratios experienced by vehicles and animals for different atmospheric conditions, adapted from Tennekes (2009)

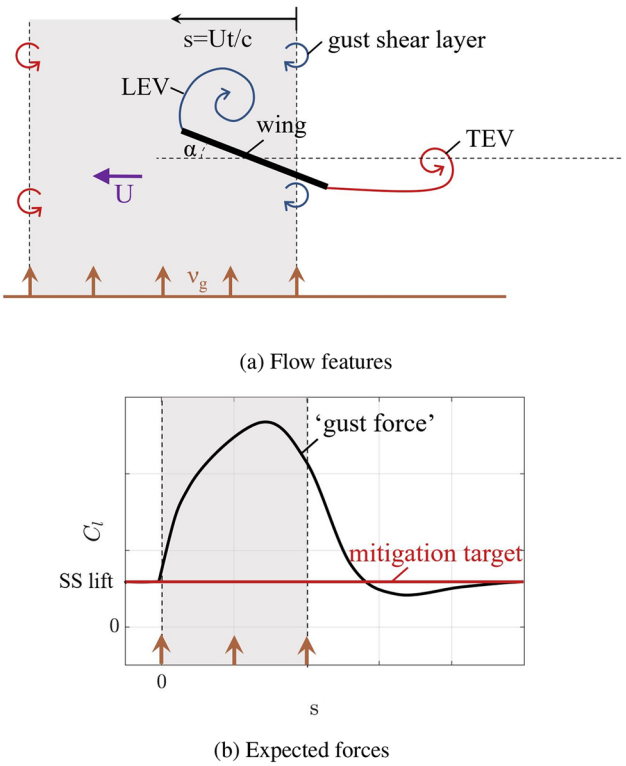

Fig. 2 Characteristics of a wing-gust encounter at an angle of attack

Recent experiments have shown that the effect of a large-amplitude transverse gust can be completely mitigated with a pitch motion determined empirically by trial and error (Andreu-Angulo and Babinsky 2020). A similar mitigation profile has also been calculated directly by a low-order model (Andreu-Angulo and Babinsky 2022) that makes use of Wagner (Wagner 1925) and Küssner (Küssner 1930) theories. In addition, the flow physics that characterise the mitigation wing-gust encounter have been carefully analysed (Sedky et al. 2022). These studies demonstrated that a wing pitch motion can be successful at mitigating the loads produced by a high-amplitude gust. In addition, the correct pitch mitigation profile can be determined from relatively simple classical models, which include assumptions that may appear unsuitable at first but become applicable at low effective angles of attack. This work has only been demonstrated for wings producing zero lift before encountering a gust, where the incoming flow at least is in the linear regime. In reality, a wing is expected to produce lift, which is likely to make the problem more complex and moved it away from the assumptions made in the classical theories. The work presented here, therefore, analyses the mitigation approach for instances where the wing is producing lift at a non-zero angle of attack before entering the gust. This asymmetry now permits to make a distinction between upwards and downwards gusts.

1.1 Problem set up

The fluid dynamics of vehicle-gust interactions are extremely complex. To study the fundamental effects governing this interaction, we simplify the geometries and consider only two-dimensional flow, as outlined in Fig. 2a. The wing of an aerial vehicle is represented with a thin rectangular plate that travels at constant speed U towards a high GR transverse gust. The flat plate is a common representation for wings in unsteady low Re aerodynamics, where the flow is typically separated (Eldredge and Jones 2019). The case of a wing with separated flow is frequently harder to treat in low-order models, and thus, in the present study, the separated case is useful to study the limitations of the gust mitigation approach. Other aerofoils shapes at low angles of attack are considered a simpler test scenario. Given the nature of this problem and the theory used, we consider that this work can be extrapolated to those simpler cases while its limitations emerge from the most separated flows, as discussed at the end of this paper. Another advantage of studies on flat plates is that the flow is relatively insensitive to Re variations in the 10^5 regime.

The position of the wing relative to the gust is given by the non-dimensional quantity $s = Ut/c$, where $s = 0$ corresponds to the wing leading edge entering the gust, t is time, and c is the wing chord length. The experimental gust replicates a top-hat edge shape with approximately constant transverse velocity v_g inside, and zero v_g outside. This gust profile is selected due to its extreme unsteady effects and large loads (Andreu-Angulo et al. 2020). The objective of this study is to mitigate this strong load and maintain a constant lift force for the entire wing-gust encounter, as shown in Fig. 2. The study will be performed for initial angles of attack, $\alpha_o = \alpha(s \leqslant 0)$, of 0°, 10°, and 20° on upwards and downwards gusts. In addition, experiments on upwards gusts

at $\alpha_o = 45°$ are performed to analyse the limits for high effective angles of attack. The initial angle of attack determines the steady-state lift, C_{lss}, that is to be maintained during the gust encounter.

An example of the measured gust velocity profile is given in Fig. 3b. This gust replicates the desired top-hat shape except for a smeared transition at the edges and some fluctuations inside the gust. The wing motion used to mitigate the gust perturbation is a one-degree-of-freedom pitch about the wing mid-chord as shown in Fig. 3a. This approach provides a simple test case to explore the mitigation model. Subsequent investigations may then focus on other pitch locations, flaps, or more complex types of controls. Given that we explore large gust ratios, the mitigating pitch motions likely include large amplitudes and frequencies. This itself generates large unsteady forces, and consequently, the prediction of the required pitch profile is complicated.

2 Model for mitigation pitch profile

In order to mitigate the gust loads on wings at different angles of attack, we follow the approach described in Andreu-Angulo and Babinsky (2022). They used a low-order model based on conventional unsteady aerodynamics to determine a pitch motion that alleviates the forces experienced during a transverse gust encounter. However, this study was confined to the simplest case of a flat plate wing operating at zero incidence. In general, a wing carries lift throughout a gust encounter, which raises the question about the suitability of such a gust mitigation approach for wings operating under lifting conditions, particularly around the stall boundary. Furthermore, lifting wings can experience both upwards and downwards gusts, with the latter often being considered more dangerous. The present article focuses on these topics. To analyse the lifting wing cases, the original theory from Andreu-Angulo and Babinsky (2022) requires the modifications summarised in this section.

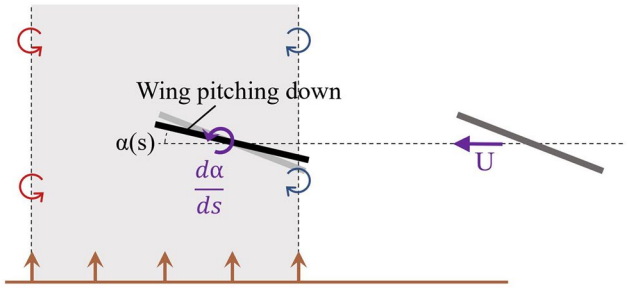

(a) Mitigation strategy - pitch motion

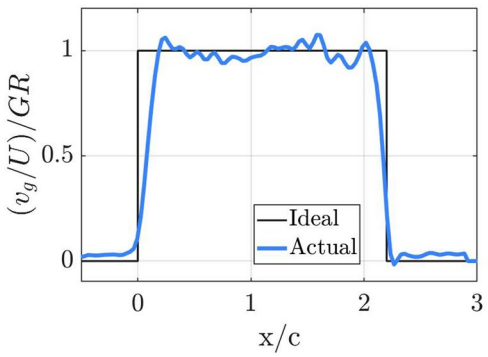

(b) External perturbation - gust

Fig. 3 Elements of the pitching wing-gust encounter

To model the complex flow, several assumptions are made. These assumptions are commonly used in unsteady aerodynamic theories with considerable success (Eldredge 2019; Baik et al. 2012; McGowan et al. 2011).

- The flow is considered to be inviscid and incompressible.
- The vorticity elements shed from the wing trailing edge are confined to the horizontal plane.
- Vorticity is not shed from the leading edge.
- The disturbances affecting the wing are small, and thus, small-angle approximations are valid.

These assumptions allow for a simple relation between the wing lift and the flow velocity perpendicular to the wing $v(x, k)$ in the frequency domain (Theodorsen 1940; Gülçat 2010),

$$C_l(k) = \underbrace{-2C(k)\int_{-1}^{1}\sqrt{\frac{1+x^*}{1-x^*}}\frac{v(x^*,k)}{U}\mathrm{d}x^*}_{\text{Circulatory}} \underbrace{-2\int_{-1}^{1}\sqrt{1-x^{*2}}\frac{v'(x^*,k)}{U}\mathrm{d}x^*}_{\text{Non-circulatory}} \tag{1}$$

where k is the oscillation frequency, and C(k) is known as the Theodorsen's function, which is composed of Hankel functions (Theodorsen 1940). In addition, x^* is the location along the wing chord and v is the flow velocity at the location x^*. The first integral in equation (1) corresponds to the circulatory term. This force component ensues from the shedding of vorticity from the wing. The second term is non-circulatory and is calculated from the derivative of the wing-normal flow v'. This force contribution arises from the vorticity evolution in the wing boundary layer that is not associated with any shed vorticity (Corkery et al. 2019). Equation (1) can be used to calculate the total lift force on a

wing for different wing-normal velocity perturbations. In our study, this perturbation is a result of the fast pitch motions and the sharp changes in the gust velocity impinging on the wing. Because the lift is linearly related to the wing normal flow velocity, v, the different contributions of lift can be calculated independently and combined at the end.

2.1 Circulatory Wagner component—wing motion

The force experienced during a wing gust encounter can be divided into the effect from the wing motion and from the gust. Each of these includes a circulatory and non-circulatory force component as shown in Eq. ((1)). The circulatory force of an impulsively started pitching wing can be calculated from the first term on the right of Eq. (1), as shown by Wagner (1925) in the time domain. The circulatory lift response (assuming $\sin\alpha = \alpha$) for this case is, according to Gülçat (2010),

$$C_l^W(s) = 2\pi\alpha W(s) \tag{2}$$

This result is similar to the steady equation for C_l but with an added transient effect expressed by the Wagner function $W(s)$. A wing starting from rest eventually reaches a steady-state lift of $C_{lss} = 2\pi\alpha_o$. In the current study, we use an approximation of the Wagner function proposed by Garrick Garrick (1938),

$$W(s) = 1 - \frac{1}{2+s} \tag{3}$$

The Wagner solution accurately described the unsteady force experienced by small impulsive changes in angle of attack. However, we are interested in an arbitrary pitch motion. To model this, the analytical lift force due to a step change in the wing motion can be linearly superimposed to recreate any motion. The lift coefficient at the location s is calculated by summing the response of all the incremental pitch motions that have influenced the wing at previous time steps (Andreu-Angulo and Babinsky 2022). This is achieved mathematically with a Duhamel's integral (Anderson 2015),

$$\begin{aligned} C_l^W(s) = {} & 2\pi W(0)\left(\alpha(s) + \frac{1}{4}\frac{d\alpha(s)}{\mathrm{d}s}\right) \\ & + 2\pi\int_0^s \frac{dW(\tau)}{d\tau}\left(\alpha(s-\tau) + \frac{1}{4}\frac{d\alpha(s-\tau)}{ds}\right)d\tau \end{aligned} \tag{4}$$

where $\alpha(s-\tau)$ is the angle of attack at the location $s-\tau$. Note once more that the wing pitches about the mid chord while the no through flow condition is enforced at the three quarter chord point. The term $\frac{1}{4}\frac{d\alpha(s)}{\mathrm{d}s}$ accounts for the rotational velocity contribution at the three quarter chord. Equation (4) is the final expression for the circulatory lift on a wing pitching about the mid chord following an arbitrary motion $\alpha(s)$.

2.2 'Added Mass' component—wing motion

In addition to circulatory effects, an unsteady wing motion also experiences non-circulatory, or 'added mass', forces. The 'added mass' force is directly related to time variations of the velocity distribution along the chord due to wing motions $\frac{\mathrm{d}v}{\mathrm{d}t}$ (Brennen 1982). Substituting the wing-normal flow distribution along a wing pitching about its half-chord and travelling at a constant speed results in the 'added mass' expression (Limacher et al. 2018; Limacher 2021; Andreu-Angulo 2022),

$$C_l^{am}(s) = \frac{\pi}{2}\left(\cos^2(\alpha(s)) - \sin^2(\alpha(s))\right)\frac{d\alpha(s)}{\mathrm{d}s} \tag{5}$$

which shows that the non-circulatory force is dependent on the angle of attack and the pitch rate. Prior to entering the gust, the pitch rate is zero, and therefore, there is no 'added mass' force. Once the wing starts to pitch inside the gust, this force component becomes substantial. This force component accounts for the effect of large angles of attack, which is considered the most appropriate for gust mitigation applications, as explained in (Andreu-Angulo and Babinsky 2022).

2.3 Küssner component—gust interaction

The last major contribution to the lift arises from the gust flow impinging on the wing. Küssner used a very similar approach to Wagner to find an analytical solution for a wing experiencing a transverse step gust (Küssner 1930, 1932). The main difference between this scenario and Wagner's impulsive pitch motion is that the gust flow affects the wing progressively while wing motions have a uniform effect across the chord. This permits to readily calculate the circulatory and non-circulatory components in one term. In addition to the previous assumptions, the gust shear layer is considered rigid so that it does not deflect during the wing-gust encounter. The effects of gust shear layer deflection on the total loads have been measured to be small (Gehlert et al. 2021). The predicted lift response for a sharp-edged gust is (Leishman 2000),

$$C_l^K(s) = 2\pi\frac{v_g}{U}K(s) \tag{6}$$

where $\frac{v_g}{U}$ is effectively the angle of attack induced by the gust. This solution, therefore, diverges from the steady result by the transient Küssner function. The complex Küssner response can be approximated with a simpler function (Bisplinghoff et al. 1955),

$$K(s) = \frac{4s^2 + 2s}{4s^2 + 5.64s + 0.8} \tag{7}$$

While simple, the Küssner model has been shown to accurately predict the transient wing force in a wide variety of gust encounters (Andreu-Angulo et al. 2020). The solution is however derived for a wing at zero degrees angle of attack. In the current study, large geometric angles of attack need to be modelled in order to mitigate the effects of high-amplitude gusts. This requires some adjustments to the original theory, such as the introduction of the additional term $D_c = \frac{c}{2}(1 - \cos(\alpha))$, as described in Andreu-Angulo and Babinsky (2022). Lastly, an arbitrary gust velocity profile and wing motion can again be modelled by using a Duhamel's integral similar to equation (4). The final lift force contribution due to an arbitrary transverse gust velocity profile is,

$$C_l^K(s) = 2\pi \int_0^s \frac{dK(\tau)}{d\tau} \frac{v_g(s - \tau - D_c(s - \tau))}{U} \cos(\alpha(s - \tau))\, d\tau \tag{8}$$

The basic Küssner additional gust force from equation (6) is not affected by having a nonzero α_o. However, the adjustments to include high angles of attack were initially derived assuming $\alpha(s) \leqslant 0$, while in the current study $\alpha(s)$ can also be positive. Fortunately, all the trigonometric terms in Eq. (8) are cosines and independent of the sign of α. Moreover, the $D_c(s - \tau)$ and $\cos(\alpha(s - \tau))$ continue to be valid.

2.4 Unsteady mitigation model

The total lift force during a pitching wing-gust encounter becomes a combination of the circulatory component of the Wagner model, the 'added mass' term due to the wing pitch motion, and the Küssner force adjusted for a wing at high angles of attack. These components arise from different wing-normal velocity distributions and can be linearly combined due to the direct relation between C_l and v / v' shown in Eq. (1). These first order terms account for most of the wing loads during gust mitigation, even for high amplitudes, as concluded in Andreu-Angulo and Babinsky (2022). The result for the unsteady model used in this work is consequently a combination of equations (4), (5), and (8). This equation is used to calculate the pitch profile, $\alpha(s)$, that results in a constant lift value. The constant value is given by the initial lift, $C_{lss} = 2\pi\alpha_o$, which can be substituted in order to obtain,

$$\begin{aligned}\alpha_o =& W(0)\left(\alpha(s) + \frac{1}{4}\frac{d\alpha(s)}{ds}\right) \\ &+ \underbrace{\int_0^s \frac{dW(\tau)}{d\tau}\left(\alpha(s-\tau) + \frac{1}{4}\frac{d\alpha(s-\tau)}{ds}\right)}_{\text{Wagner circulatory}} \\ &+ \underbrace{\frac{dK(\tau)}{d\tau}\frac{v_g(s-\tau - D_c(s-\tau))}{U}\cos(\alpha(s-\tau))\, d\tau}_{\text{Kussner adjusted}} \\ &+ \underbrace{\frac{1}{4}\left(\cos^2(\alpha(s)) - \sin^2(\alpha(s))\right)\frac{d\alpha(s)}{ds}}_{\text{Pitch non-circulatory}}\end{aligned} \tag{9}$$

Equation (9) provides a direct relation between the lift, the angle of attack, and the transverse gust velocity. The desired pitch kinematics to achieve a target lift force can now be determined using an iterative approach, which is shown schematically in Fig. 4. Here, the lift coefficient is calculated for one time step t and compared with the desired lift ($2\pi\alpha_o$). If C_l is within a designed error (set to 0.01 in our case) of $C_l^{desired}$, the computation progresses to the next step. Otherwise, α is corrected by a value proportional to the difference $-(C_l - C_l^{desired})$, which converges the results due to the direct relation between α and C_l. A new C_l is calculated for the corrected α and the process is repeated until C_l is within 0.01 of $C_l^{desired}$, at which point the calculation progresses to the next step $t + dt$. For the current study, a convergence study showed that a dt of 0.02 s produced accurate results.

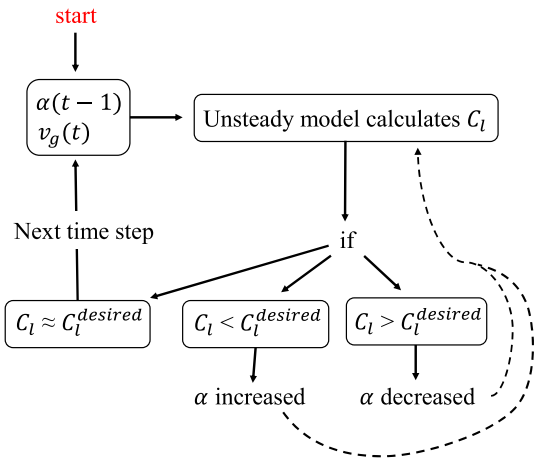

Fig. 4 Diagram of the iterative approach to calculate the mitigation pitch profile

3 Experimental methodology

The wing-gust interaction is studied experimentally to evaluate the potential of the proposed mitigation strategy. The experiments are performed in the $9 \times 1 \times 1$ m water tow tank at the University of Cambridge. In this facility, models are towed through stationary water. The absence of a free stream flow permits the implementation of an undisturbed cross flow to recreate the gust. In addition, more accurate force measurements can be achieved in water due to scaling effects, which results in forces approximately 4 times larger than in air for the same flow conditions. The Reynolds number for the experiments is 25,000 based on the model chord. The tow velocity (0.24 m/s) is determined using an electro-optical position sensor with a resolution of 1 mm that is mounted on the side of the carriage. The model used in these experiments is a glass plate with a chord length of 0.12 m, a span of 0.48 m, and a thickness of 0.004 m. The model is oriented vertically in the tank with its lower end free and its top end flush with a skim plate to effectively double its aspect ratio, as shown in Fig. 5. The top end is directly connected to the force balance.

In order to create the top-hat gust, a rig is assembled inside the tow tank test section to generate a cross-flow in the direction perpendicular to tow. The wing travels at a distance of 200 mm from the gust rig outlet and the gust rig pump motor RPM is adjusted to achieve the desired gust velocity confirmed by particle image velocimetry (PIV) measurements. More information regarding the gust rig can be found in Corkery et al. (2018). The gust velocity profile is assumed to be equal to the gust flow measured in the absence of the wing, while in a realistic application, the gust might be determined from real-time measurements some distance upstream. However, measurements have shown that the gust velocity measured as near as one chord length upstream of the wing leading edge was not affected by the presence of the wing (Andreu-Angulo and Babinsky 2022), which justifies the use of the gust-only velocity profile (as seen in Fig. 3b) as input for the calculation of the mitigation motion.

3.1 Pitch motion

To achieve the desired pitch motions, the wing mid-chord is bolted into a shaft connected to a Maxon EC-45 brushless motor, as shown in Fig. 6a. Two bearings on either side of the shaft are used to reduce vibrations. The motor shaft is attached to a 74:1 gearbox which increases the torque and gives greater control during the pitch manoeuvres. The motion is measured with an encoder hosted inside the motor that has a precision greater than 0.01 degrees. A positional EPOS-4 controller is used to actuate the motor to the desired pitch profile.

The measured gust velocity profile shown in Fig. 3b is substituted into Eq. (9) to calculate the unsteady pitch profiles. The results for the three initial angles of attack, α_o, are shown in Fig. 6b for upwards and downwards gusts with a $GR = 0.5$. In addition, this figure also includes the pitch

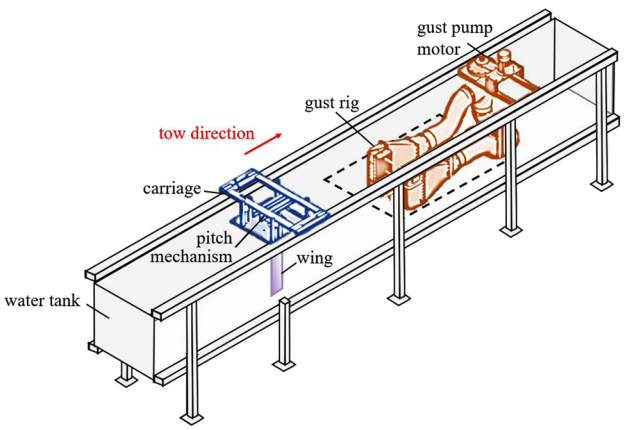

Fig. 5 Water towing tank

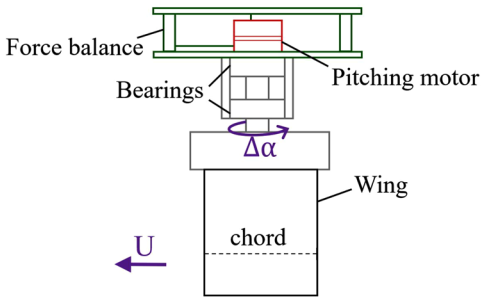

(a) Side view of set-up for the pitching mechanism

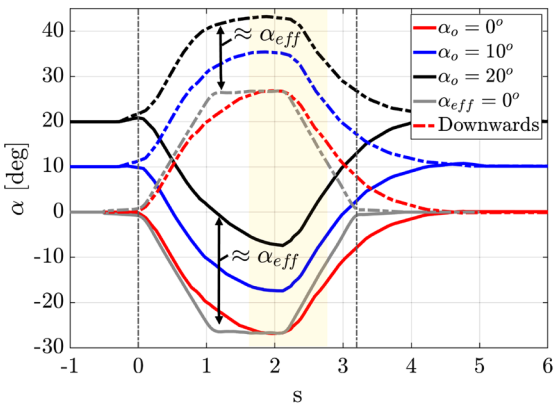

(b) Mitigation pitch motions calculated by the unsteady model for upwards (solid) and downwards gusts (dashed)

Fig. 6 Pitch motion characteristics

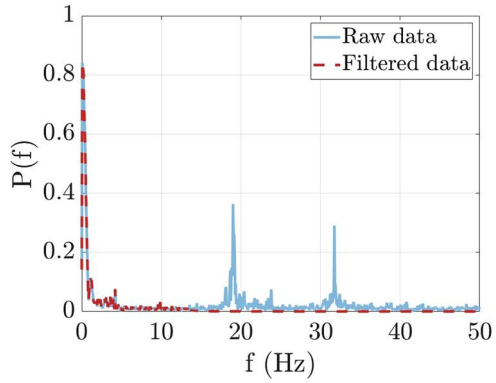

(a) Fast fourier transform of force data

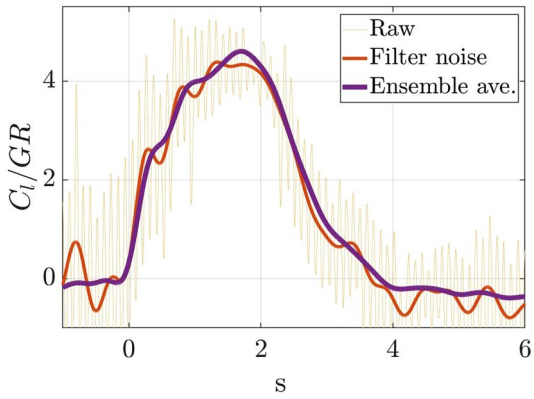

(b) Force data filtering for $GR = 0.5$

Fig. 7 Force data analysis

profiles that would maintain a zero effective angle of attack. The difference between the coloured and grey curves effectively visualises the wing α_{eff} for the pitching cases. All pitch profiles present a maximum magnitude at $s/c = 2.2$ and have a relatively similar shape for different α_os.

3.2 Force measurements

The stream-normal and streamwise wing load components are acquired using a two-component force balance at a sampling frequency of 1 kHz. Each of the two components is measured by a load cell with a range of ± 50 N and a resolution of 0.01 N. The stream-normal force data are normalized by the dynamic pressure and the wing area in order to calculate the coefficient of lift. The raw signal exhibits large amplitude noise at 19 Hz, as seen in Fig. 7a. Therefore, a low-pass bidirectional filter with a cut-off frequency of 18 Hz is applied to the signal. Afterwards, the result from five runs is ensemble averaged. The lift coefficient curves resulting from the various levels of filtering are shown in Fig. 7b.

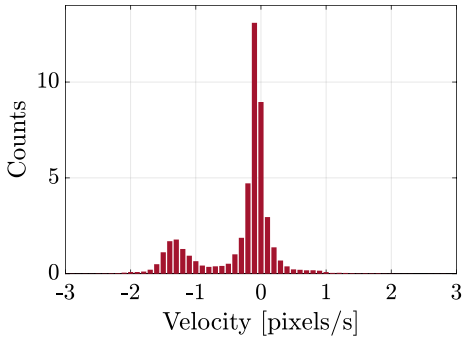

Fig. 8 Particle displacement histogram

The force uncertainty due to cell cross-talk and offset loading is determined below 2% when ensemble averaging data from 5 runs (Corkery 2018).

3.3 Particle image velocimetry

Planar time-resolved PIV data are acquired using the two camera set-up shown in Fig. 5. A high-speed Nd:YLF 527nm laser creates a beam pulsing at a frequency of 0.2 kHz that is transformed into a laser sheet through a set of optics. The laser sheet has a thickness of about 2 mm and illuminates titanium dioxide seeding particles placed in the flow. The entire flow field around the wing can be

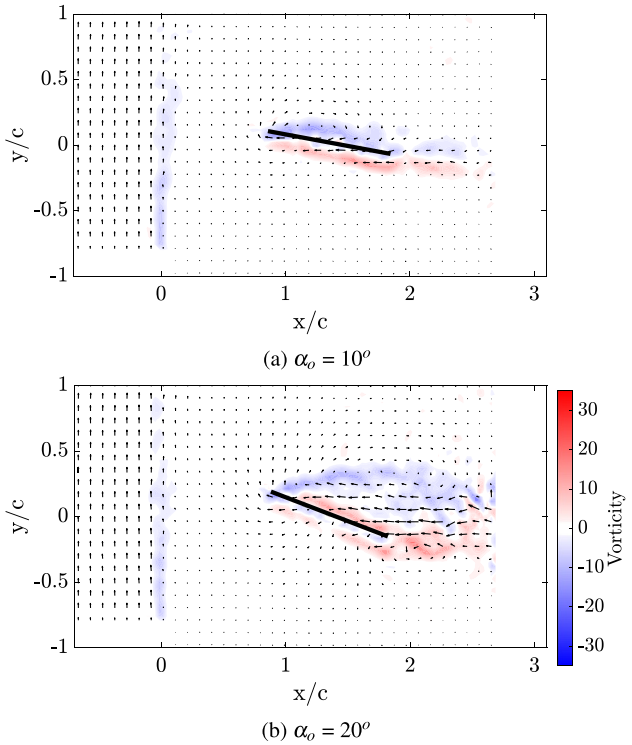

(a) $\alpha_o = 10^o$

(b) $\alpha_o = 20^o$

Fig. 9 Flow behind the wing prior to entering the gust

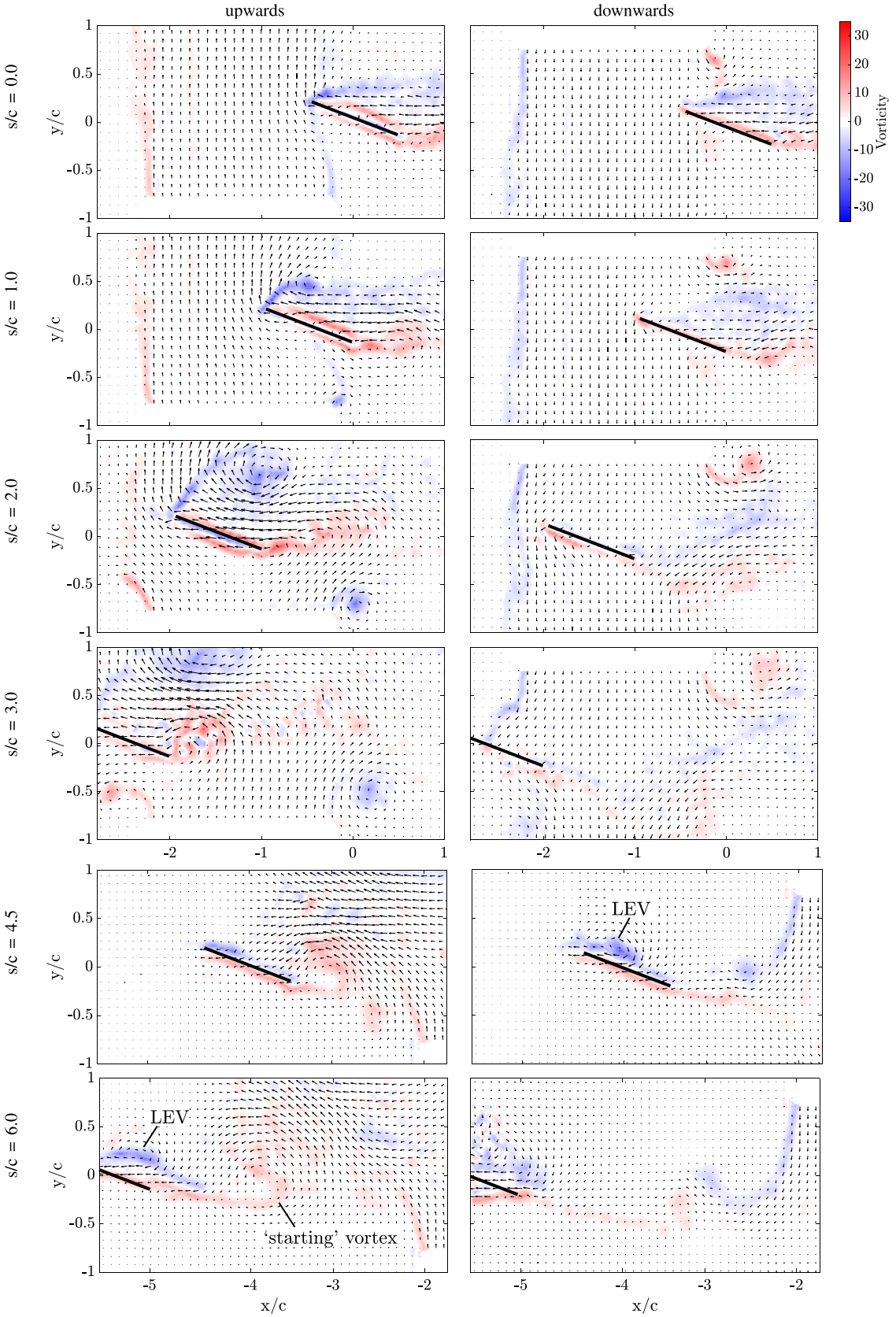

Fig. 10 Flow evolution for upwards and downwards wing-gust encounters, $GR = 0.5\ \alpha_o = 20°$

resolved thanks to the use of glass, which permits the laser light to pass through the model. At the same time, surface reflections are reduced. The particle data are collected by two cameras with a resolution of 1280×800 pixels that are synchronised with the laser using a programmable timing unit PTU-X from Davis (LaVision). The field of view of the first camera resolves the data on the wing upper surface, while the second camera is positioned to measure the data on the lower surface. Using the DaVis software, the images from both cameras are later processed and stitched together to obtain the final velocity fields.

The experimental error associated with PIV is calculated in the DaVis software, which uses the approach described in Wieneke (2015) and Sciacchitano et al. (2015). The maximum uncertainty in the region of interest is calculated to be below 8% for one run. The results are averaged over 5 runs to reduce this uncertainty to $U/\sqrt{N}$ 3.5%. This uncertainty calculation does not account for systematic errors, such as "peak-locking". When "peak-locking" occurs, measured velocities are biased towards integer values in terms of pixels per second (Raffel et al. 2007). To verify that "peak-locking" is avoided, the probability density function is computed to ensure that particle velocities corresponding to fractions of a pixel are measured. The results are shown in Fig. 8, for which the peak at 1.3 pixels/second corresponds to the gust velocity. The absence of spikes at non-zero integer values confirms that peak locking does not occur.

4 Gust only case—no mitigation

Before attempting pitch motions, unmitigated wing-gust encounters are examined. In this case, the wing maintains a constant angle of attack α_o as it encounters the gust. The results shown are for a gust ratio of 0.5, which increases the wing's effective angle of attack by 26.5° when the gust is upwards and decreases it by the same amount when the gust is downwards.

Prior to the gust, a flat plate towed at non-zero angle of attack generally experiences vorticity shedding from its sharp leading and trailing edges, which produces a wake and these are considerable start-up transient. Therefore, the wing is towed for 15 chords before encountering the gust so the wake is fully developed. The size of the wake increases with angle of attack, as seen in Fig. 9. For $\alpha_o = 10°$, the wake is relatively thin with mostly attached flow similar to $\alpha_o = 0°$ (Andreu-Angulo and Babinsky 2022), while for $\alpha_o = 20°$ the flow is clearly separated. Because of its difference to previous studies at zero incidence, the following discussion mainly concentrates on the 20 degrees case.

4.1 Upwards gust

As seen in Fig. 10, when a wing at $\alpha = 20°$ enters an upwards gust, the vorticity shed from the leading edge rolls into a LEV on the wing upper surface. The LEV separates from the wing surface relatively quickly. At the same time, vorticity shed from the TE remains planar until the effect of the LEV separation pushes it closer to the wing upper surface. During gust exit, $s/c = 3.0$, the flowfield observed prior to the encounter does not resume immediately. Instead, at $s/c = 4.5$, the flow is mostly attached. Farther away from the gust, at $s/c = 6$, there is evidence that the wing sheds a new starting TE vortex and a secondary LEV. These vortices are expected to eventually advect away allowing the steady-state flow observed in Fig. 9 to re-establish. This flow behaviour is qualitatively similar to that described for a wing at zero degrees incidence in a previous study (Andreu-Angulo and Babinsky 2022). The main differences are that, in the $\alpha_o = 0°$ case, the primary LEV stays attached longer and the secondary LEV does not emerge.

4.2 Downwards gusts

The flat plate at $\alpha = 20°$ encountering a downwards gust experiences a decrease in its effective angle of attack. This causes a significantly different flow evolution compared to the upwards gusts, as shown in Fig. 10. During gust entry, the downwards gust flow impinges on the separated upper surface of the wing, 'pushing' the separated wake away from the wing. The gust influence then reduces vorticity shedding from the wing due to the lowering of α_{eff}. For the $\alpha_o = 20°$ and $GR = 0.5$ case, the effective angle of attack inside the gust is only 6.5°. Consequently, the flow is predominantly attached. After exiting the gust, the vorticity shedding does not resume straight away. Instead, similar to the upwards gust case, a LEV (shown in Fig. 10) develops on the upper surface and eventually sheds.

The flow for the $\alpha_o = 0°$ case encountering a downwards gust is the inverted version of the upwards gust in Fig. 11. Here, the effective angle of attack is −26.5° and thus the flow separates and a LEV is shed from the wing surface. In addition, the wing does not experience a secondary LEV.

4.3 Lift response

The lift responses for upwards wing-gust encounters at four angles of attack are compared in Fig. 12. Prior to the gust, the wing experiences a constant steady-state lift, C_{lss}, whose value depends on the angle of attack. At low α_o, the magnitude of C_{lss} is consistent with the theoretical result $2\pi\alpha$,

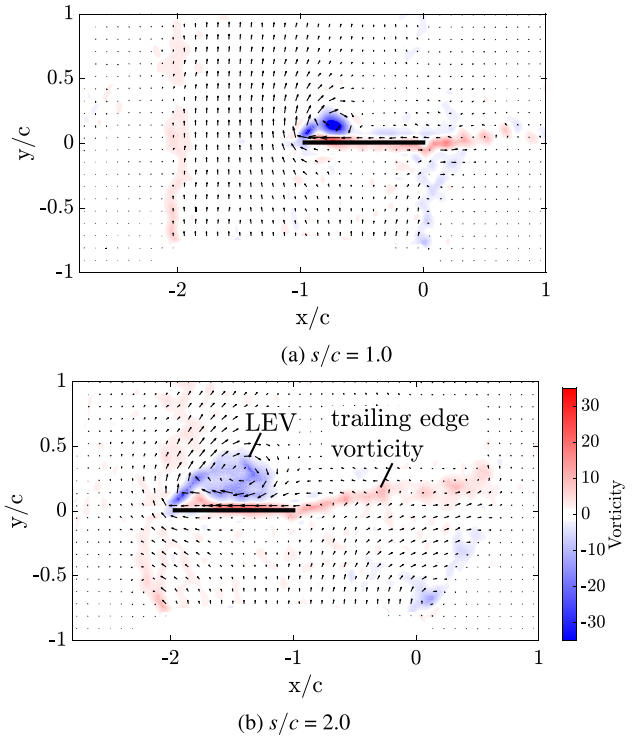

Fig. 11 Flow around a wing-gust encounter at $GR = 0.5\alpha = 0^o$, after Andreu-Angulo and Babinsky (2022)

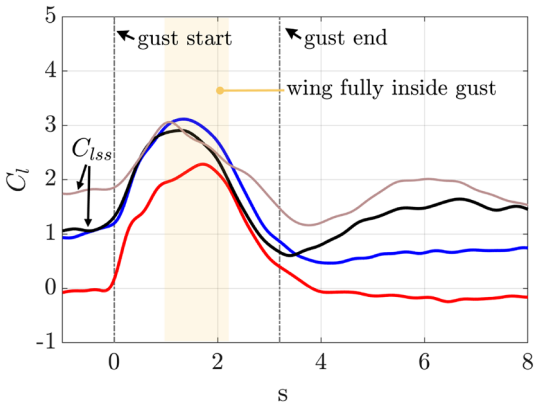

Fig. 12 Lift response for an upwards $GR = 0.5$ gusts

which assumes attached flow. However, at high α, where the flow is clearly separated, the steady-state lift is below $2\pi\alpha$. As the wing enters the gust, the lift magnitude increases for all incidences. The lift response produces a spike centred around $s/c = 1.5$, after which the lift decreases. After gust exit, the lift magnitude eventually returns to the steady-state value. The maximum lift value does not exceed $C_l = 3.2$ for any angle of attack.

The results can be compared further by considering exclusively the additional lift produced by the gust

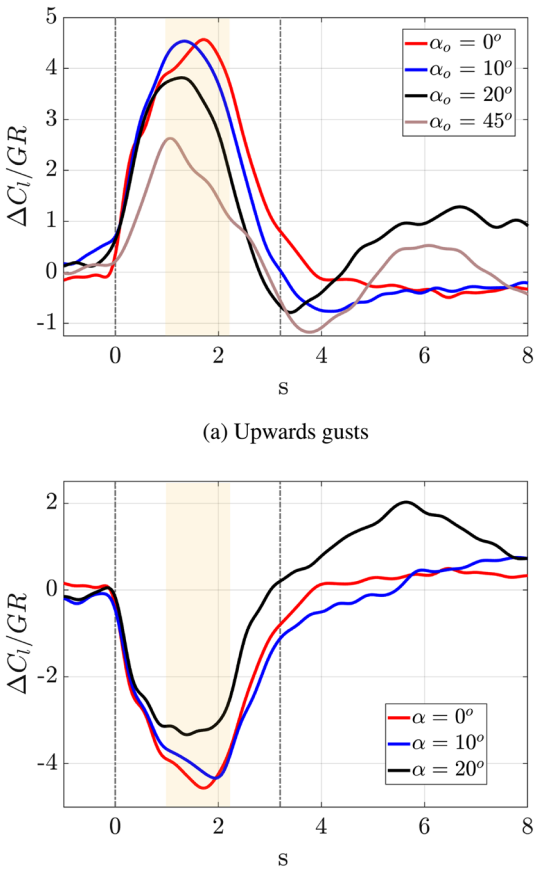

Fig. 13 Normalised responses for gust-only cases $GR = 0.5$ gusts

$\Delta C_l = C_l - C_{lss}$, as shown in Fig. 13a. In addition, the loads are normalised by the gust ratio in order to facilitate future GR comparisons. There is a lower and earlier maximum additional lift for greater angles of attack. The value of $\Delta C_{lmax}/GR$ decreases from 4.6 to 2.6 as α_o increases from 0° to 45°. Another large difference in lift for the four angles of attack is observed after gust exit, where the $\alpha_o = 20°$ and 45° cases experience a large secondary lift peak.

The lift characteristics can be explained by some of the flow features. The smaller and earlier ΔC_l peak for the greater α_o is associated with a faster detachment of the LEV from the wing surface. This LEV detachment results in a decrease in lift. The flow evolution also explains the wing lift response after exiting the gust. The lower α cases experience attached flow before and after the gust and show only small lift variations for $s/c > 5$, but remaining close to the steady-state values. The $\alpha = 20°$ case presents separated flow before entering the gust attached flow soon after exiting. Attached flow is expected to produce higher lift and thus Fig. 13a shows higher ΔC_l after exiting the gust ($s/c > 5$)

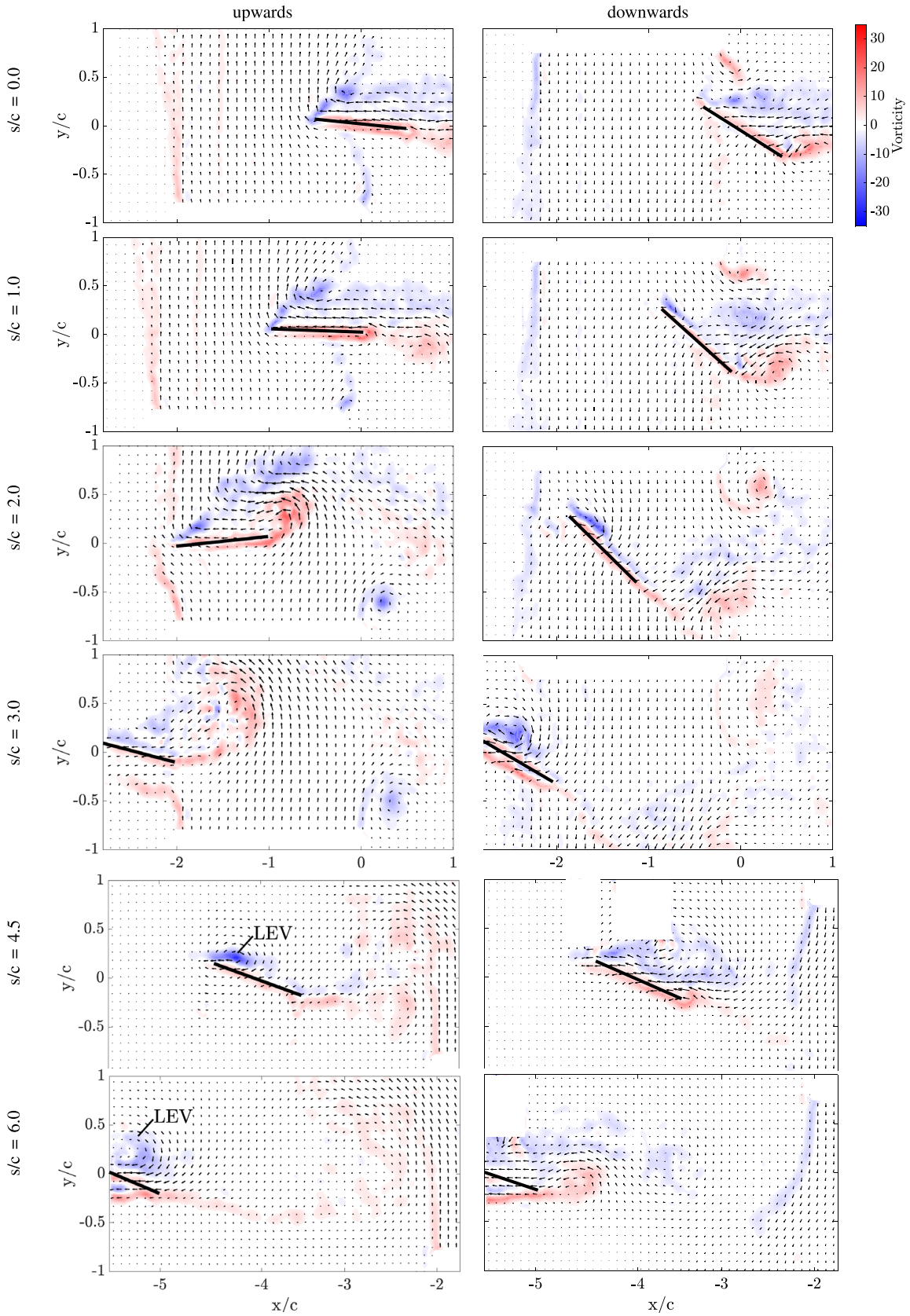

Fig. 14 Flow evolution around a wing pitching to mitigate upwards and downwards gusts, *GR*=0.5

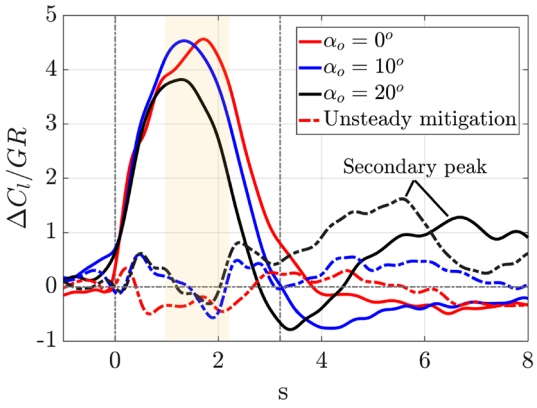

(a) Upwards gusts

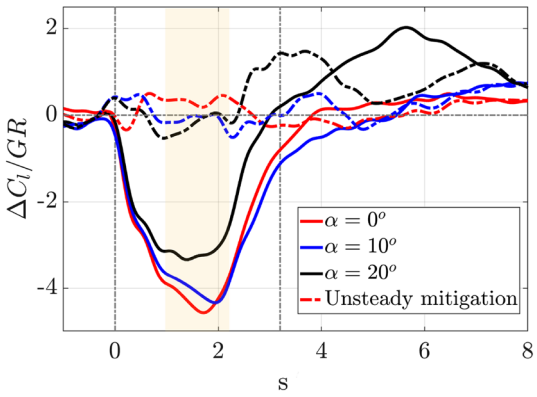

(b) Downwards gusts

Fig. 15 Lift mitigation at different initial angles of attack

than before entering. Eventually, the flow around the wing sheds a LEV and separates, causing the lift to return to its steady-state value.

Normalised additional lift results for the downwards gust case are displayed in Fig. 13b. The state of the wing before entering the gusts is independent of gust direction, and therefore, the steady-state lift on the wing is the same for upwards and downwards gusts. However, as the wing enters the downwards gust, it experiences a decrease in lift, or a negative ΔC_l spike. The magnitude of this spike, $|\Delta C_{lmax}|$, decreases with increasing angle of attack. Afterwards, all cases present a lift increase near gust exit, at around $s/c = 2.2$. When the wing exits the gust, the lift continues to increase back to the steady-state value. Similar to the upwards gusts, the lift for the $\alpha_o = 20°$ case experiences a secondary lift peak near $s/c = 5$ due to the unsteady shedding of vorticity.

Table 1 Mitigation effectiveness for *GR* 0.5

	$\alpha_o = 0°$ (%)	$\alpha_o = 10°$ (%)	$\alpha_o = 20°$ (%)
Upwards	90	87	79
Downwards	89	88	84

5 Mitigation results

In order to mitigate the gust-induced lift spikes, the wing is rotated according to the pitch profiles calculated by the low order model and shown in Fig. 6b. Even though model assumptions are broken, prior studies have demonstrated lift mitigation at large *GR*s where the unsteady model can not accurately predict the gust-only loads (Andreu-Angulo and Babinsky 2022). This was explained by the fact that, in order to maintain zero lift, the effective angle of attack is kept small by the mitigating pitch, thus keeping the actual flowfield within the small angle assumption. However, here we investigate gust encounters where the initial angle of attack is non-zero and where the model assumptions are already broken even before the gust encounter (e.g. at 20° incidence where the wing is stalled).

5.1 Upwards gust

In order to maintain constant lift for the upwards gust encounter, the wing starts to pitch down as it enters the gust, as shown on the left column of Fig. 14. Nevertheless, the wing continues to experience a relatively large α_{eff} throughout the gust encounter, approximately 26.5° at $s/c = 1.0$. This results in significant vorticity shedding from the leading edge. The wing also sheds vorticity from the trailing edge, which rolls into the upper surface. After exiting the gust, the wing returns to the initial angle of attack at around $s/c = 4.5$. At this time, the wing undergoes a LEV shedding process that eventually develops into the detached flow seen prior to gust entry, similar to the gust-only cases.

5.2 Downwards gust

Figure 14 also shows the flow around a wing that pitches upwards to mitigate a downwards gust. The increase in α produces a small LEV on the wing's upper surface, which stays attached to the wing during the entire gust encounter. The wing pitches back down when exiting the gust at $s/c = 2.2$, producing more leading-edge vorticity. Consequently, at $s/c = 4.5$, a LEV is developed and starts to separate. This contrasts with the upwards and gust-only results, where the LEV at this time is just starting to form.

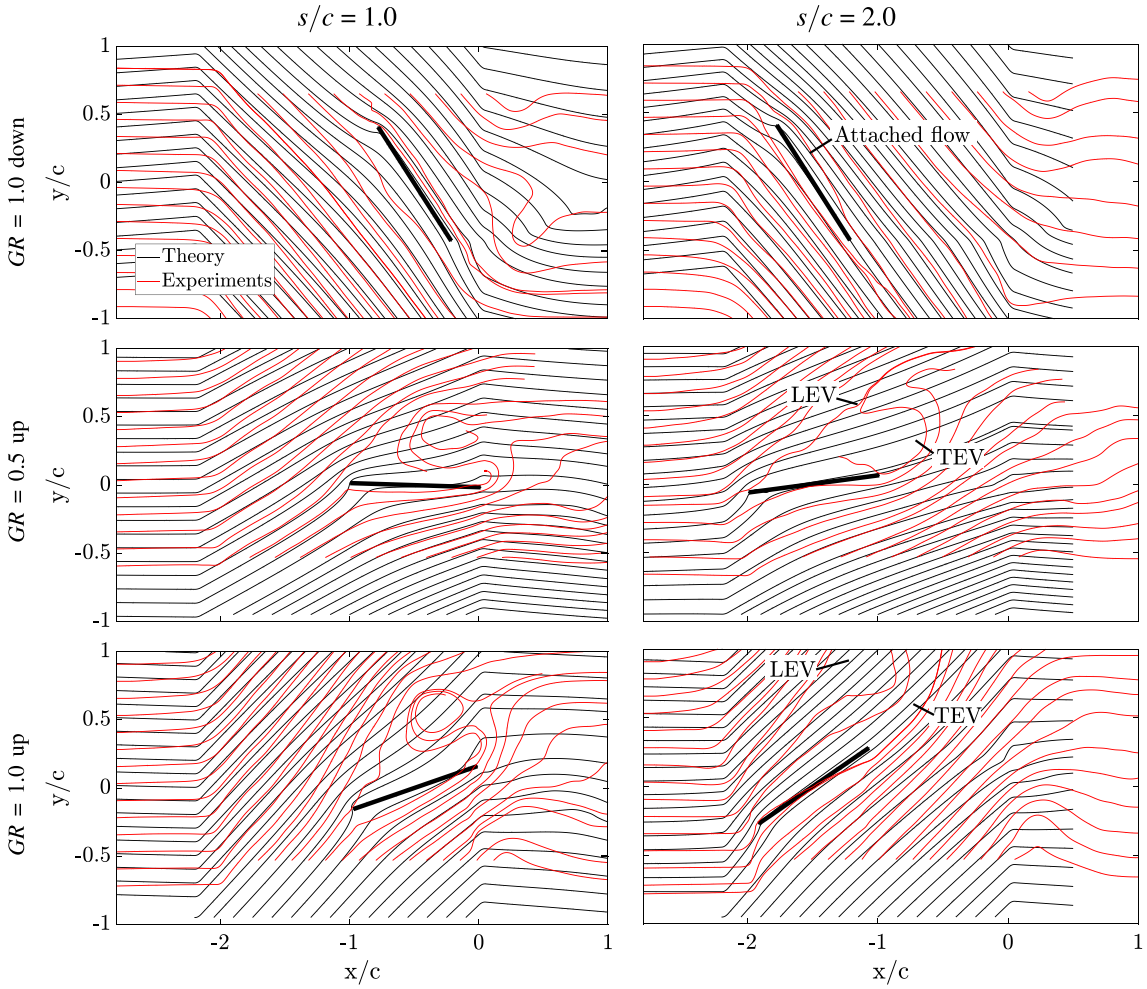

Fig. 16 Theoretical and measured streamlines around various pitching wing-gust encounters, $\alpha_o = 20°$

5.3 Force mitigation

The normalised additional lift curves for these mitigation experiments are plotted together with the gust-only results in Fig. 15a. Similar to previous studies (Andreu-Angulo and Babinsky 2022), the results generally demonstrate adequate mitigation of the gust lift spike. The lift variations about C_{lss} are small and relatively random within the gust region. However, after exiting the gust, the secondary lift spike is still present for $\alpha_o = 20°$. For the mitigation experiments, the pitch action has shifted the secondary lift peak to $s/c = 5.5$ but it did not alleviate the magnitude. The mitigation model ignores LE vorticity shedding and thus the secondary lift peak, which is affected by this shedding, is not treated.

The mitigation approach is also successful in alleviating the primary downwards gust force spike, as shown in Fig. 15b. The lift stays within $-0.5 < C_l < 0.5$ of the target value when the wing is inside the gust. After exiting the gust, the mitigation pitch motion is once again unsuccessful at removing the secondary lift peak in the $\alpha_o = 20°$ case. However, there is a shift to earlier s/c in the appearance of this feature and a slight reduction in its magnitude. This earlier peak is attributed to the earlier development and shedding of the LEV after gust exit. Nevertheless, the dangerous negative lift spike caused by downwards gusts is well mitigated by this model-based approach.

A more quantitative assessment of the load mitigation can be calculated from the maximum lift values with and without pitch control. The percentage mitigation value is calculated from the difference between the baseline and the control lift peak,

$$M_{\%} = \frac{C^g_{lmax} - C^m_{lmax}}{C^g_{lmax} - C_{lss}} \tag{10}$$

where C^g_{lmax} is the maximum lift in the gust-only case and C^m_{lmax} is the maximum lift in the mitigation case. The mitigation effectiveness of the primary lift peak for different

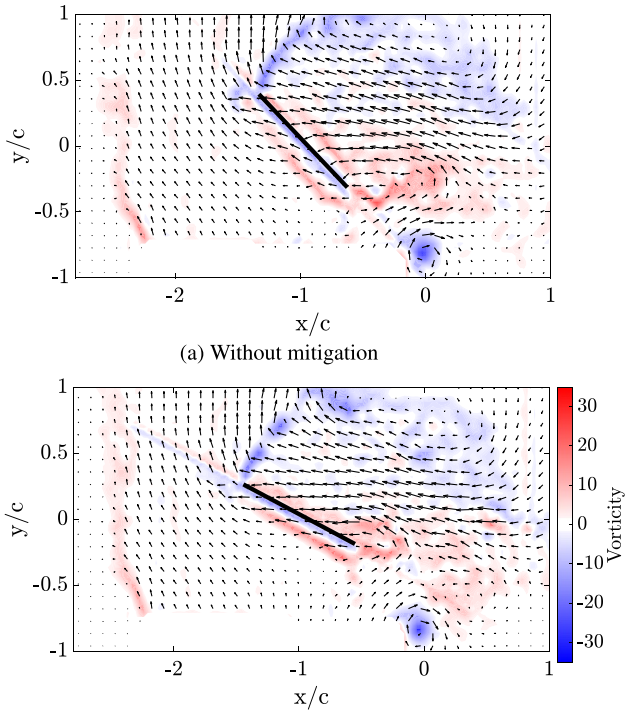

(a) Without mitigation

(b) With mitigation

Fig. 17 Flow around a wing at large $\alpha_o = 45°$ encountering a $GR = 0.5$ gust

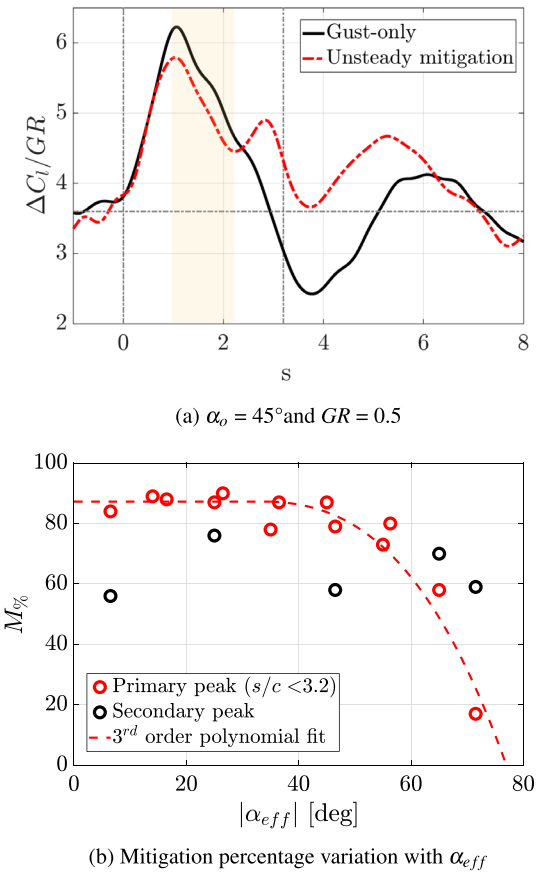

(a) $\alpha_o = 45°$and $GR = 0.5$

(b) Mitigation percentage variation with α_{eff}

Fig. 18 Limitations of the mitigation approach

cases is presented in Table 1. good mitigation of around 80–90%—a reduction in peak load by a factor of 5–10—in all cases. When including the secondary lift peak, $M_{\%}$ for $\alpha_o = 20°$ decreases to 58 % and 56 % for upwards and downwards gusts, respectively.

5.4 Streamlines

The effectiveness of the mitigation approach for upwards and downwards gusts is analysed further by comparing the experimental and theoretical streamlines. The theoretical streamlines are those predicted by the model from equation (9) used for mitigation. The first row in Fig. 16 shows the results around a wing pitching to mitigate a $GR = 1.0$ downwards gust. The results for the $GR = 0.5$ case are very similar and therefore omitted in the interest of brevity. The streamlines present a close match between the experiments and the theory. In both, the flow travels parallel to the wing due to the small effective angle of attack.

The second and third rows in Fig. 16 display a wing encountering an upwards $GR = 0.5$ and $GR = 1.0$ gust respectively. The experimental streamlines for both cases present a clear LEV that causes a similar amount of curvature in the flow. However, at s/c=1.0, the LEV in the $GR = 1.0$ case is about 0.2 chords farther away from the wing surface. At $s/c = 2.0$, the streamline curvature produced by the LEV remains relatively close to the wing for the $GR = 0.5$ case. The match between experiments and theory is worse than in the downwards case, and this is accompanied by a decrease in mitigation effectiveness to 79 %. For $GR = 1.0$, the difference between the theoretical and experimental streamlines is greater than for $GR = 0.5$ case due to the LEV advecting upwards and leaving the field of view. This causes a further reduction of the mitigation effectiveness to 58 %. These results demonstrate that it takes a significant divergence of the flow physics from the theoretical assumptions before the mitigation effectiveness reduces below 80 %.

5.5 Main limitations of the mitigation approach

The mitigation errors at large α_{eff} are expected due to the assumptions embedded in the model, such as small perturbations and no shedding from the leading edge. A pitching wing-gust encounter with characteristics very distant from the model assumptions is shown in Fig. 17b. Here, the wing travels initially at 45° and pitches following the unsteady model to mitigate a $GR = 0.5$ transverse gust. Taking into account α_o and α_{ind}, the maximum effective angle of attack for the gust-only case is 71.5°. The flow is highly separated

throughout the gust encounter for the unmitigated and mitigated cases shown in Fig. 17. This flow is significantly different to other mitigation cases, where a small LEV stays close to the wing's surface and the wing pitches to negative angles of attack.

The pitch motion for this extreme case does not mitigate the gust loads, as shown in Fig. 18a, only reducing the maximum lift by 17 %. Interestingly, the most significant difference between the gust-only and mitigation cases occurs after exiting the gust. The mitigation lift response does not present the negative peak at $s/c = 3.7$. The lift results indicate that the mitigation approach is inappropriate for this wing-gust encounter.

In order to explore the limits of the mitigation approach, the mitigation effectiveness $M_{\%}$ of the unsteady pitch profile is plotted in Fig. 18b for the cases from this study and those in Andreu-Angulo and Babinsky (2022). These results are plotted versus the absolute maximum α_{eff} for the gust-only case. It can be seen that the mitigation is strong (typically above 85 %) for cases where $|\alpha_{eff}| < 60°$. The mitigation strategy is therefore robust for a large range of angles of attack, but it drops sharply for $|\alpha_{eff}| > 60°$. The equivalent of $M_{\%}$ where a significant secondary peak was observed the mitigation effectiveness for this feature is also shown by black markers. This confirms that the approach is not well suited to mitigation of this feature, and the secondary peak is responsible for the greatest errors when $|\alpha_{eff}|$ remains below 60 degrees.

6 Conclusions

A pitching wing entering a high-amplitude top-hat gust is studied experimentally. The wing is towed at a constant angle of attack to produce a steady-state lift before encountering the gust, which can be upwards or downwards. The encounter is characterised by a large lift spike and unsteady flow. In order to alleviate the lift spike, the wing is pitched to create a force that counteracts the gust force. The appropriate pitch motion is calculated using a theoretical model based on classical unsteady theory. The results demonstrate the capability of this approach to mitigate gust loads on wings up to relatively high α_{eff}.

- For an upwards gust encounter without mitigation, increasing the initial wing angle of attack promotes separation and results in a lower maximum lift.
- Downwards gusts suppress vorticity shedding for the wing leading edge due to the reduction in the wing α_{eff}. Therefore, the LEV evolution differs greatly from an upwards gust, but the relative lift peak magnitude is only slightly smaller.
- Wings at α_o that produces highly separated flows ($\alpha_o > 10°$) experience a secondary lift peak after exiting the gust. This peak is due to the flow around the wing being attached right after gust exit. Subsequently, a LEV emerges and shed before the wing returns to the separated steady state.
- The mitigation approach is successful in most of the cases presented. Lift mitigation of approximately 85% is observed when the wing does not exceed an effective angle of attack of $\pm 60°$ in the gust-only case.
- The largest mitigation error typically occurs at the secondary peak after the wing has exited the gust. The model requires improvements to be capable of mitigating this specific condition.
- Generally, downwards gusts are more easily mitigated than upwards gusts. This is associated with the smaller effective angle of attack due to the mitigation action.

Author contributions IA performed the experiments from this study, developed the mitigation approach, analysed the results, and wrote the manuscript. HB envisioned the overall path of the project, helped analyse the results and reviewed the manuscript.

Funding The authors would like to thank the Cambridge Trust for financial support. Moreover, the project that gave rise to these results received the support of a fellowship from the "la Caixa" Foundation (ID 100010434). The fellowship code is LCF/BQ/EU21/11890135.

Declarations

Conflict of interest The authors are not aware of any competing interests of financial or personal nature related to the work presented.

Ethical approval Not applicable.

References

Anderson JD (2015) Fundamentals of aerodynamics, vol 1. McGraw-Hill, London (**1011.1669v3**)

Andreu-Angulo I (2022) Mitigation of gust loads through pitching. PhD thesis, University of Cambridge

Andreu-Angulo I, Babinsky H (2020) Negating gust effects by actively pitching a wing. In: AIAA aerospace sciences meeting, 2020, Orlando, Florida, pp 1–15, https://doi.org/10.2514/6.2020-1057
Andreu-Angulo I, Babinsky H (2022) Mitigation of airfoil gust loads through pitch. AIAA J 60(9):5273–5285. https://doi.org/10.2514/1.j061348
Andreu-Angulo I, Babinsky H, Biler H, Sedky G, Jones AR (2020) Effect of transverse gust velocity profiles. AIAA J 10(2514/1):J059665
Baik YS, Bernal LP, Granlund K, Ol MV (2012) Unsteady force generation and vortex dynamics of pitching and plunging aerofoils. J Fluid Mech 709:37–68. https://doi.org/10.1017/jfm.2012.318
Biler H, Badrya C, Jones AR (2019) Experimental and computational investigation of transverse gust encounters. AIAA J 57(11):4608–4622. https://doi.org/10.2514/1.j057646
Bisplinghoff RL, Ashley H, Halfman RL (1955) Aeroelasticity. Addison-Wesley, Cambridge
Brennen CE (1982) A review of the added mass and fluid inertial forces. Tech. Rep. CR 82.010, Naval Civil Engineering Laboratory
Cheney JA, Stevenson JP, Durston NE, Song J, Usherwood JR, Bomphrey RJ, Windsor SP (2020) Bird wings act as a suspension system that rejects gusts: Bird wings act as a suspension system. Proc R Soc B Biol Sci. https://doi.org/10.1098/rspb.2020.1748rspb20201748
Corkery SJ (2018) Unsteady aerodynamics of wing gust encounters. PhD thesis, The University of Cambridge
Corkery SJ, Babinsky H, Harvey JK (2018) On the development and early observations from a towing tank-based transverse wing-gust encounter test rig. Exp Fluids. https://doi.org/10.1007/s00348-018-2586-0
Corkery SJ, Babinsky H, Graham WR (2019) Quantification of added-mass effects using particle image velocimetry data for a translating and rotating flat plate. J Fluid Mech 870:492–518. https://doi.org/10.1017/jfm.2019.231
Eldredge JD (2019) Mathematical modeling of unsteady inviscid flows. Springer, Berlin
Eldredge JD, Jones AR (2019) Leading-edge vortices: mechanics and modeling. Annu Rev Fluid Mech 51:75–104. https://doi.org/10.1146/annurev-fluid-010518-040334
Fuller JR (2008) Evolution of airplane gust loads design requirements. J Aircr 32(2):235–246. https://doi.org/10.2514/3.46709
Garrick L (1938) On Some reciprocal relations in the theory of nonstationary flows. Tech, Rep, p 629
Gehlert P, Andreu-Angulo I, Babinsky H (2021) Unsteady vorticity force decomposition-evaluating gust distortion. In: AIAA Scitech 2021 Forum, pp 1–23, doi: https://doi.org/10.2514/6.2021-1084
Gülçat Ü (2010) Fundamentals of modern unsteady aerodynamics. Springer, Berlin
Küssner HG (1930) Untersuchung der bewegung einer platte beim eintrill in eine strahlgrenze. Luftfahrtforschung p 425
Küssner HG (1932) Stresses produced in airplane wings by gusts. Tech. rep., NACA TM654, Springfiled, VA
Leishman JG (2000) Principles of helicopter aerodynamics, 2nd edn. Cambridge University Press, Cambridge
Limacher E, Morton C, Wood D (2018) Generalized derivation of the added-mass and circulatory forces for viscous flows. Phys Rev Fluids 3(1):1–25. https://doi.org/10.1103/PhysRevFluids.3.014701
Limacher EJ (2021) Added-mass force on elliptic airfoils. J Fluid Mech 926:1–12. https://doi.org/10.1017/jfm.2021.741
McGowan GZ, Granlund K, Ol MV, Gopalarathnam A, Edwards JR (2011) Investigations of lift-based pitch-plunge equivalence for airfoils at low Reynolds numbers. AIAA J 49(7):1511–1524. https://doi.org/10.2514/1.J050924
Raffel M, Willert CE, Wereley ST, Kompenhans J (2007) Particle image velocimetry: a practical guide. Springer, Berlin
Roberts D, Hunt G (1968) Measurements of transient pressures on a narrow-delta wing due to a vertical gust. Tech. Rep. 1012, http://repository.tudelft.nl/view/aereports/uuid:52c20ef3-bf3c-4bd3-a0f5-65d4be94b193/
Sciacchitano A, Neal DR, Smith BL, Warner SO, Vlachos PP, Wieneke B, Scarano F (2015) Collaborative framework for PIV uncertainty quantification: comparative assessment of methods. Meas Sci Technol. https://doi.org/10.1088/0957-0233/26/7/074004
Sedky G, Gementzopoulos A, Andreu-Angulo I, Lagor FD, Jones AR (2022) Physics of gust response mitigation in open-loop pitching manoeuvres. J Fluid Mech 944:1–29. https://doi.org/10.1017/jfm.2022.509
Tennekes H (2009) The simple science of flight. The MIT Press, Boston
Theodorsen T (1940) General theory of aerodynamic instability and the mechanism of flutter. Tech. Rep. 496, NACA
Vance JT, Faruque I, Humbert JS (2013) Kinematic strategies for mitigating gust perturbations in insects. Bioinsp Biomimetics. https://doi.org/10.1088/1748-3182/8/1/016004
Wagner H (1925) Über die Entstehung des dynamischen Auftriebes von Tragflügeln. J Appl Math Mech 5(1):17–35. https://doi.org/10.1002/zamm.19250050103
Watkins S, Milbank J, Loxton BJ, Melbourne WH (2006) Atmospheric winds and their implications for microair vehicles. AIAA J 44(11):2591–2600. https://doi.org/10.2514/1.22670
Wieneke B (2015) PIV uncertainty quantification from correlation statistics. Meas Sci Technol. https://doi.org/10.1088/0957-0233/26/7/074002

I. Andreu-Angulo recently graduated from the University of Cambridge with his work on wing-gust interactions and gust mitigation techniques. His focus are unsteady aerodynamics and vehicle design. He has now joined Emirates Team New Zealand as a Fluid Dynamics Engineer to help defend the 37th Americas Cup.

H. Babinsky researches fundamental and applied aerodynamics with application to aerospace, transport and energy production. Particular focus areas are transonic/supersonic flows, unsteady aerodynamics and road vehicles. His research is predominantly experimental but includes theoretical and numerical studies in collaboration with other groups across the globe.